Air-Sea Exchange: Physics, Chemistry and Dynamics

Edited by

G.L. Geernaert

Kluwer Academic Publishers

Chapter 9

EXCHANGE MEASUREMENTS ABOVE THE AIR-SEA INTERFACE USING AN AIRCRAFT

CHRISTOPHER A. VOGEL
Atmospheric Turbulence and Diffusion Division
National Oceanic and Atmospheric Administration
Oak Ridge, TN

TIMOTHY L. CRAWFORD
Field Research Division
National Oceanic and Atmospheric Administration
Idaho Falls, ID

9.1 Introduction

Relative to measuring exchange rates on fixed platforms over land the measurement of fluxes over the open sea involves additional challenges including adequately handling platform motion and maintaining measurement systems in harsh environments. However, we are approaching an era where, given the advancements in instrument technology and processing speed, these sorts of measurements are becoming increasingly routine. Through a number of past experiments (see Smith et al. 1996 for a summary of recent studies) at fixed locations we have begun to quantify momentum, moisture and heat fluxes directly above the air-sea interface in a variety of conditions and have addressed the underlying physics responsible. A strength of these studies is their ability to measure over continuous periods allowing the assessment of temporal variabilities. Since ultimately a goal is to routinely monitor air-surface exchange on a global scale through remote sensing from spaceborne platforms, a logical progression has been to address how representative point measurements are to a region of the size, for example, of a large scale numerical model grid or of a satellite pixel (often of the order 10^3-10^5 km^2). An obvious candidate for assessing such representativeness is the aircraft, and although a number of investigators have measured fluxes within the atmospheric boundary layer (Lenshow 1972; Lenshow et al. 1980, 1981; Dejardins et

G.L. Geernaert (ed.), Air-Sea Exchange: Physics, Chemistry and Dynamics, 231–245.

al. 1982, 1989; Hacker, Schwerdtfeger 1988) using aircraft to probe the marine atmospheric surface layer is relatively new.

Because of the resolution needed in the turbulent fluctuations of the winds accurate platform removal is critical when using an aircraft for air-surface exchange measurements. Also, due to the scales of turbulence responsible for transporting momentum and scalars, spatial measurements must often be accomplished on scales of the order of a meter. Further, due to the inherent flux divergences as one moves away from the air-sea interface, there is the challenge of accomplishing the measurements within the marine atmospheric surface layer, often only a few hundred meters thick. And there are the challenges of making the measurements in flow that is undisturbed by the aircraft itself. In short, one desires an aircraft which can safely fly relatively low and slow, with a clean profile immediately ahead of the aircraft, containing highly accurate platform motion sensing capabilities, and equipped with fast-response measurement systems (Crawford et al. 1996).

The NOAA Atmospheric Turbulence and Diffusion Division began developing a mobile flux (MFP) system mounted on an airborne platform in the early 1990s (Crawford et al., 1990). Through a number of years of refinement it has now become a reliable and accurate means of determining the spatial variability of fluxes within the atmospheric surface layer. The primary aircraft chosen for these measurements has been a Rutan-design Long-EZ experimental aircraft, a platform well-suited for surface layer measurements. This aircraft can fly stably at 15 m height above underlying terrain or seas and fly at ground speeds of 50 m/s. It is a "pusher" design with the engine and propeller at the rear allowing for a clean profile through the air. Turbulent fluctuations can be sampled at 50 Hz allowing spatial measurements on the order of 1 meter. Simultaneous use of both a differential and absolute global positioning system (GPS) allows for highly accurate position and velocity measurements of the platform itself in order to separate the apparent airflow measurements from the actual instantaneous winds.

9.2 The Mobile Flux Platform

The Mobile Flux Platform was designed as a strap down wind measurement system intended to be mounted on a variety of vehicles (i.e., aircraft and watercraft) and to primarily measure atmospheric turbulent structure and scalar exchange. The platform was developed in response to research needs for a low-cost system capable of measuring representativeness and spatial variability of air-surface exchange in various environments. The practical nature of the MFP was made possible by recent technological advances in both low-cost miniature sensors, GPS, and computer technology. Small sensors allowed co-location of both the air velocity and motion instruments. This in turn allows direct measurement of the motion of the turbulence probe mounted ahead of the nose of the aircraft instead of simply the vehicle motion of the aircraft itself. GPS technology allows accurate determination of sensor velocity

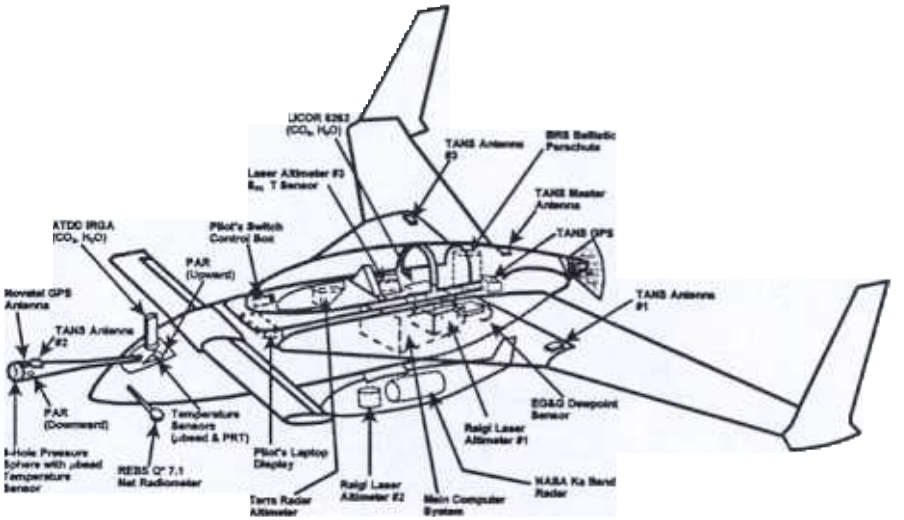

Figure 9.1 The mobile flux platform and other measurement systems as mounted on the Long-EZ research aircraft. Note the turbulence probe mounted in the "clean" airflow ahead of the nose of the aircraft. Also note the two laser altimeters mounted on the left and right strake of the aircraft, and third laser in the pod underneath the fuselage.

and position. Modern computer technology allows not only channel input, data rate, and storage flexibility, but also efficient post processing tasks such as the integration of measurements from a number of sensors used in determining the turbulent wind fluctuations and the mathematical rotation from platform to earth coordinates. Figure 9.1 gives a schematic of the MFP system and other instruments as recently mounted on the Long-EZ aircraft.

Wind measurements from aircraft are an order of magnitude more complex than from fixed sensors. This is because on the aircraft the wind vector is measured in the reference frame of the moving wind sensors and must be transformed to the reference frame of the earth. This requires measuring the sensor's velocity relative to the earth V_s as well as the air velocity relative to the sensors V_a. Thus, the determination of the actual wind vector V can be expressed through a simple summation:

$$V = V_a + V_s \qquad (9\text{-}1)$$

It is important to recognize that since the airflow sensors move significantly with respect to the airplane's center of mass these sensors define the relevant reference frame and not the aircraft itself. Also, because both the airflow measurements and the sensor velocities are large in magnitude, small errors in either can cause significant errors in the apparent wind velocities.

To overcome these potential problems several high resolution instruments are used in determining the winds. Protruding ahead of the nose of the aircraft is a turbulence

gust probe which presents a spherical face to the incident airflow. The relationship between the pressure distribution on a sphere and an incident airflow velocity vector is well known and consequently a number of pressure measurements both dynamic and static are made on the probe face. The array of pressure sensors includes types which are both differential and absolute and all are solid state in nature. Careful attention is paid to using very short distances (a few centimeters) between transducers and pressure ports so that the frequency response in the range of interest is not attenuated.

The determination of the probe velocity V_s is more complex. The fundamental approach is to use a combination of high frequency accelerometer measurements and relatively low frequency differential and absolute GPS measurements to determine the probe position and velocity with respect to the earth. Accelerometers capable of measuring accelerations in all three dimensions are mounted at the centers of mass of both the probe and the aircraft itself. The GPS system consists of both an absolute measurement system at the probe and a differential system involving the relative positions of four points on the aircraft, namely, at the probe, on each wing, and at the engine in the rear. Thus, the former system gives both the position and velocity of the probe with respect to the center of the earth, while the latter gives these quantities and additionally the angular position of the probe with respect to the aircraft itself. To determine the probe velocity V_s the accelerometers are integrated and blended with the differentiated positions and velocities given by both the absolute and differential systems. To determine the airflow velocity V_a the incident airflow velocity magnitudes are combined with the angular information given by both the relative accelerometer measurements from the probe and aircraft center of mass, and the differential GPS system. The accuracies produced through combining these measurements are ± 20 cm in position, ± 2 cm/s in velocity, and ± 0.05 degrees in orientation (heading, roll, pitch). A more detailed description of resolving the wind velocities through equation (9-1) can be found in Crawford and Dobosy (1992) and Dobosy and Crawford (1996).

Of course, the turbulent wind fluctuations are only part of the measurements needed to determine exchange rates of various scalars. For both sensible and latent heat exchange, high frequency measurements of temperature and humidity must be attained. Fast response temperature measurements are generated through a microbead thermistor mounted within the probe while water vapor and CO_2 measurements are obtained through an open-path Infrared Gas Analyzer (IRGA) designed and fabricated in-house (Auble, Meyers 1992). In addition to these measurements a host of mean measurements is also obtained including temperature, dew point, and CO_2 concentrations. In order to relate the flux magnitudes to governing processes a number of remote sensing instruments is also deployed. For air-sea work in particular important measurements include those of sea surface temperature from a downward-looking infrared sensor, and a downward-looking 3-laser array capable of resolving laser to surface distances with accuracies on the order of a millimeter.

9.3 Flux Calculations

Direct vertical flux calculations originate with high frequency measurements of vertical and horizontal winds and appropriate scalars. Mathematically, a flux F_ϕ can be expressed as:

$$F_\phi = \overline{(\rho_d w)\phi'} \qquad (9\text{-}2$$

where ρ_d is the dry air density, w is the vertical velocity and ϕ is the quantity being exchanged. The primes indicate a turbulent fluctuation implying that some mean state has been removed from the instantaneous measurements. For example, for the quantity of interest ϕ :

$$\phi' = \phi + \overline{\phi} \qquad (9\text{-}3)$$

where ϕ is the instantaneous measurement and $\overline{\phi}$ is a defined mean. For measurements obtained at a fixed point the mean is often defined as a simple time average. However, for spatial measurements especially from small aircraft near the ground it is important to employ spatial averages for most mean calculations. This arises primarily from the desire to eliminate measurement bias when the aircraft encounters updrafts or downdrafts. For example, for a fixed sampling rate, if the aircraft encounters an updraft, the pilot will decrease the angle of attack in order to maintain altitude. This will in turn cause the aircraft to increase its ground speed thereby decreasing the number of measurements for a given horizontal path. Conversely, a downdraft will cause an increase in measurements over a certain distance. Crawford et al. (1992) showed errors of 10 – 20 % in momentum, heat, moisture and CO_2 fluxes when a straight time average was used in calculating means. Thus, in calculating the turbulent fluctuations we define a mean such that

$$\overline{\phi} = \frac{1}{\overline{S}\,T} \sum \phi S \Delta t \qquad (9\text{-}4)$$

where S is the instantaneous speed of the aircraft, $\overline{S}$ the mean speed, Δt the time increment, and T the total time. Defining an appropriate mean is a critical step in determining exchange rates since the mean removal calculation is essentially applying a filter. If the filter spans too narrow a range of turbulent scales the influence of larger scale turbulence on the flux will be reduced and thus the calculated exchange rates will be underestimated. Similarly, if the filter spans too wide a range large spatial trends may artificially increase the calculated fluxes.

One method of ensuring an appropriate averaging scale is to perform cospectral analysis on the quantities of interest demonstrated in equation (9-2). As an example, Figure 9.2 shows a cospectrum of horizontal and vertical wind signals over a 16.4 km horizontal transect within a shoaling region near Duck, NC. The abscissa shows

cospectral energy multiplied by frequency while the ordinate is in normalized frequency $n = fz/S$. For this transect $z = 21.1$ m while $S = 57.1$ m/s. By examining the plot it is evident that very little energy is contributed at length scales greater than 3000 m ($n = 7.07 \times 10^{-3}$) and less than 20 m ($n = 1$). Thus, in this case we chose an averaging scale of 3000 m to use in equation (9-3) when determining the turbulent fluctuations. In employing cospectral analyses in a wide range of conditions (i.e., shallow and deep water, light and heavy seas) a choice of 3000 m for an averaging scale appears to be fairly robust (Vogel, Crawford 1996, 1997; Vogel et al. 1999). This is also consistent with previous estimates of $0.001 < n < 2$ for the range of turbulent scales contributing to transport (Kanemasu et al. 1979).

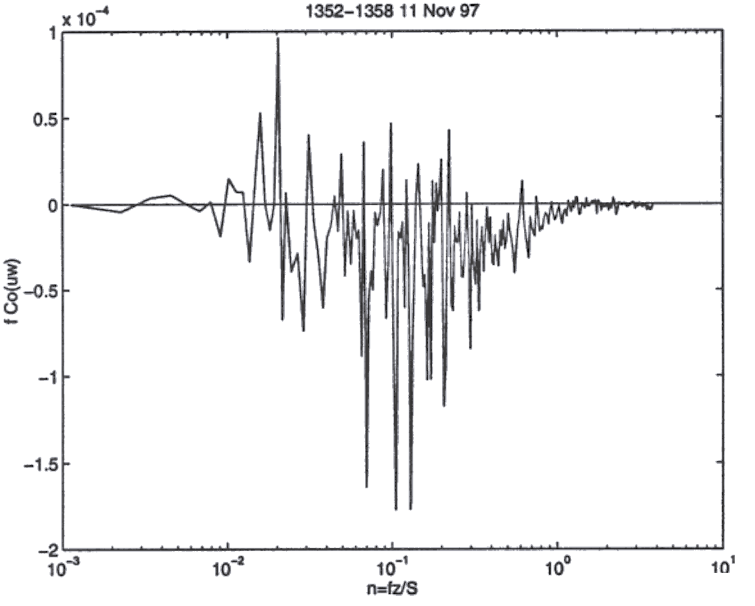

Figure 9.2 A cospectrum of horizontal and vertical wind signals for a 16.4 km transect ranging from 1 to 17 km offshore of Duck, NC. Here n is a non-dimensional frequency calculated using the frequency f, an average measurement height $z = 21.2$ m and an average aircraft ground speed $S = 57.1$ m/s. Note the relatively small amounts of energy contributed at length scales greater than 3000 m ($n = 7.07 \times 10^{-3}$) and less than 20 m ($n = 1$).

9.4 Results from Recent Experiments

The Long-EZ aircraft has recently been involved in two major air-sea interaction studies. The first, conducted in the spring of 1995, was held approximately 100 km west of Monterey, California. The second was conducted in the fall of 1997 within a shoaling region east of the Outer Banks of North Carolina. Both experiments focused

on the spatial variation of surface fluxes with an emphasis on the momentum flux. The latter experiment focused additionally on the effect of rapidly changing sea characteristics. Some results from both experiments are presented below.

9.4.1 THE MONTEREY EXPERIMENT

A primary goal of the Monterey study was to determine the magnitudes and spatial variation of the surface fluxes of momentum, heat, moisture, and CO_2. The flux measurements were conducted in conjunction with a number of separate investigations carried out aboard research vessels in the area including the naval research platform FLIP. The primary transect flown for the study involved a triangular path, shown in Figure 9.3, with the long leg centered on FLIP (Vogel, Crawford 1996). Because of the desire to also investigate the presence of atmospheric boundary-layer scale coherent structures such as roll vortices the orientation of the triangle was such that the long leg was always perpendicular to the mean wind. However, in the large majority of cases the winds were out of the northwest or west and deviations from the transect shown in Figure 9.3 were relatively small.

As an example of the flux magnitudes observed during the study Figure 9.4 shows exchange rates of momentum, sensible heat, moisture and CO_2 for a near-surface counterclockwise triangular transect (i.e., points B, C, and D in the Figure). The aircraft was flying at approximately 20 meters above the air-sea interface at a nominal ground speed of 50 m/s. Exchange rates were calculated using a 3000 m symmetrical running mean and output every 1000 m. For the long leg of the triangle, from waypoint B to waypoint C, friction velocities (equal to the square root of the downward momentum flux) are shown to be initially between 0.20 and 0.40 m/s, sensible heat fluxes are small near 10 W/m^2, moisture fluxes are near 50 W/m^2, and CO_2 exchange is downward albeit nearly negligible. As the aircraft proceeds to point C an increase in magnitude in all four exchange rates becomes apparent. In addition there is an increase in the variability. The u. values reach a maximum mean value of approximately 0.50 m/s while sensible and latent heat fluxes reach a maximum mean near 30 and 75 W/m^2 respectively. The CO_2 flux shows relatively strong uptake near 0.15 mg/m^2/s. For the transect from points C to D the magnitudes appear to slowly decrease and on the D to B transect the fluxes return to near their original values at point B. It is hypothesized that this sort of spatial variation in exchange rates is indicative of moving in and out of a coastal upwelling region.

To first order the momentum flux over the sea is governed by the mean longitudinal wind and the aerodynamic roughness length. This is apparent from the neutral wind profile relation:

$$U = \frac{u_*}{k} \ln(z/z_0) \qquad (9\text{-}5$$

where U is the mean longitudinal wind at height z, u_* the friction velocity, z_0 the aerodynamic roughness length, and k the von Karman constant. Assuming winds of 12 m/s (as shown in Figure 9.5), a measurement height of 20m, Charnock's relation

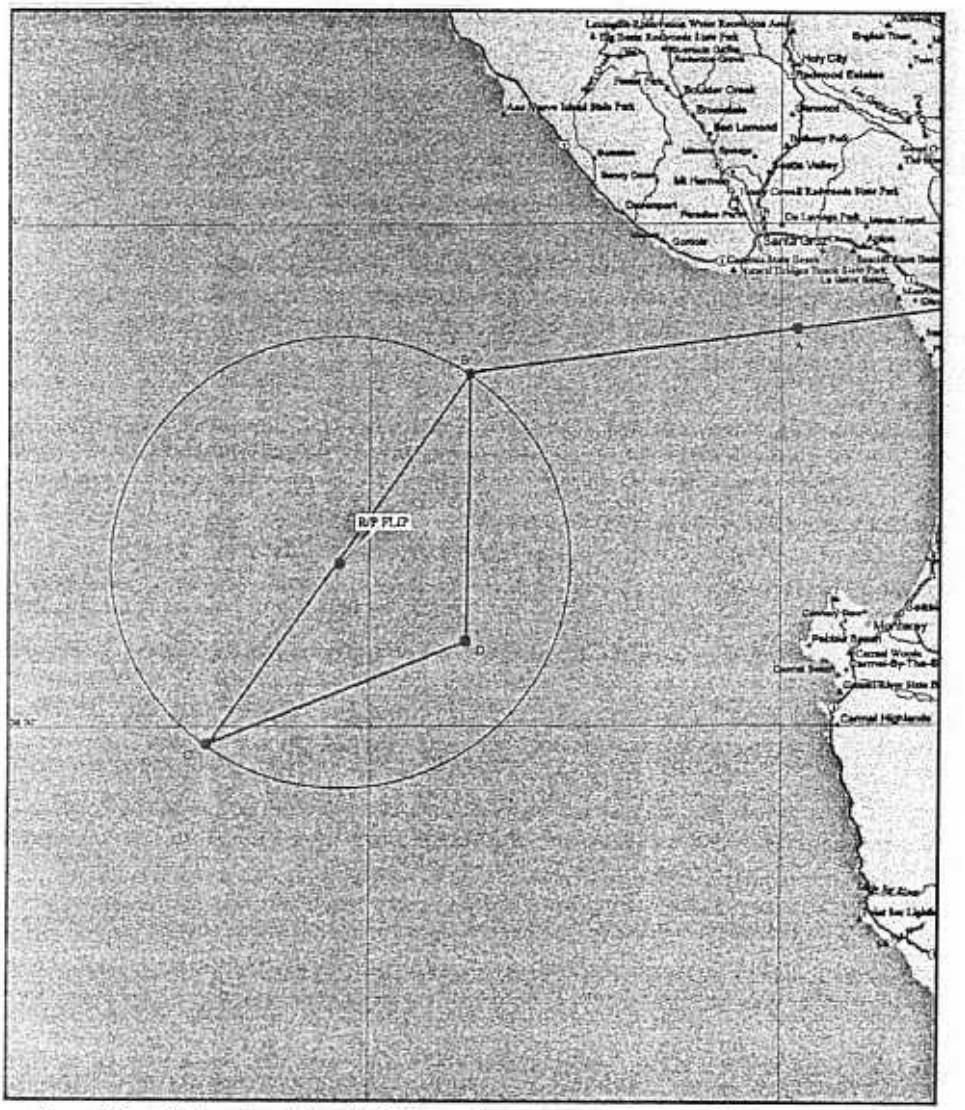

Figure 9.3 Study region during the MBL experiment in spring 1995 west of Monterey Bay. FLIP is at the center of the study region.

$z_0 = \alpha_c u_*^2 / g$ for the roughness length, and assuming values of 0.40 and 0.015 for k and α_c the Charnock constant, equation (9-5) gives a value of 0.43 for the friction velocity. These are in good agreement with values shown in Figure 9.4. Because of the small positive bouyancy flux indicated no stability corrections to (9-5) were made.

Figure 9.5 also shows changes in both the sea surface temperature and the air temperature at 20m. In particular the sea surface temperature rises significantly along

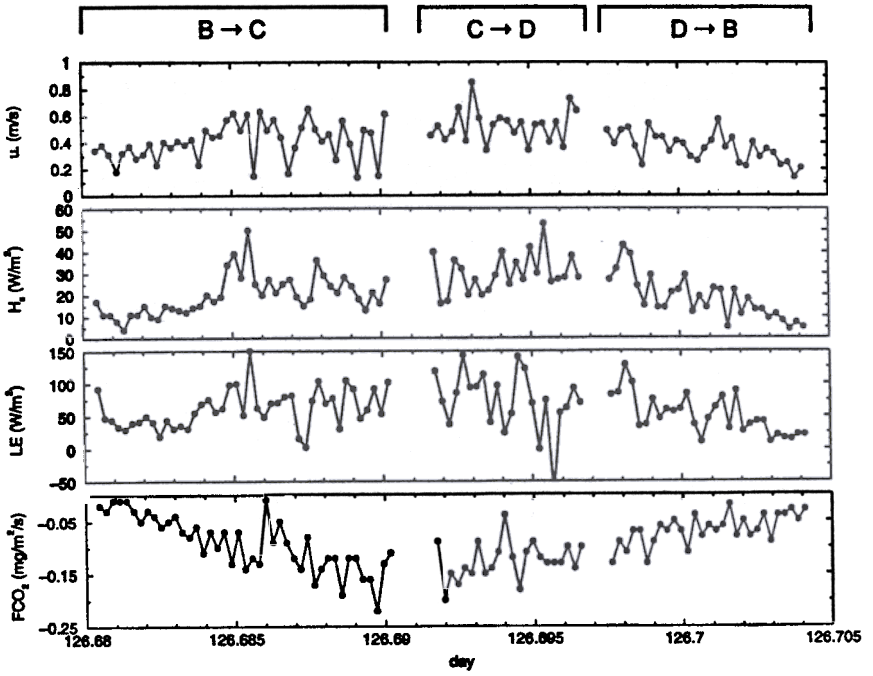

Figure 9.4 Exchange rates of the square root of momentum flux u_*, the sensible heat flux H_s, the latent heat flux *LE*, and the CO_2 flux FCO_2 around the triangular path shown in Figure 3. Note the closure in the flux variabilities as the aircraft returns to its starting position at point B.

the transect from point B to point C, and returns near its original value at the end of the D to B leg. From Monin-Obukhov similarity theory the bulk relationship for heat transfer at the sea surface can be defined as:

$$\frac{H_0}{\rho c_p} = C_H U (\theta_0 - \theta) \qquad (9\text{-}6)$$

where H_0 is the heat flux above the air-sea interface, ρ the air density, c_p the specific heat of vaporization, θ_0 the sea-surface temperature, the transect from point B to point C, and returns near its original value at the end of the D to B leg. From Monin-Obukhov similarity theory the bulk relationship for heat θ the air temperature, and C_H the transfer coefficient. Using values from Figure 9.5, substituting values for ρ and c_p, and assuming that $C_H = 1.2\ C_{DN}$, where $C_{DN} = (u_*/U)^2$ is the neutral drag coefficient, a quick calculation for the heat flux using equation (9-6) is approximately 30 W/m^2, again in good agreement with the data.

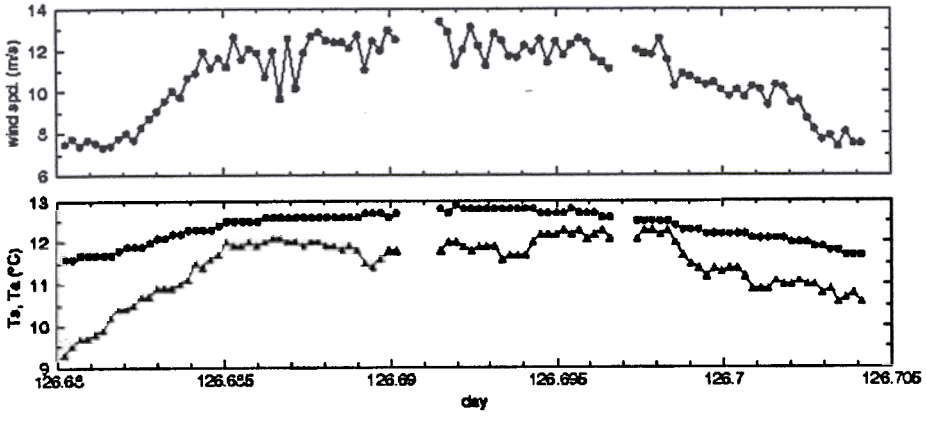

Figure 9.5 Windspeed and air-sea temperature difference measured by the aircraft during the same run as shown in Figure 9.4.

Overall, the Long-EZ aircraft flew in excess of 50 hours over a three week span. These flights covered a wide range of conditions including both low wind and high wind cases. A goal of the study was to assess the temporal and spatial variability of the momentum and scalar exchange rates. Over the course of the study the measurements ranged from 0.10 – 0.50 m/s for u_*, 0 – 30 W/m^2 for H, 0 – 120 W/m^2 for LE, and –0.13 - +0.10 mg/m^2/s for FCO_2. The spatial variation of the exchange rates both within a triangle leg and between consecutive triangle legs are given in Table 9.1 (Vogel, Crawford 1996).

Table 9-1 Spatial variation of surface exchange rates within a triangle leg and from leg to leg. The values for the within triangle leg cases are percent changes about the mean of each leg. The values for the leg to leg cases are percent changes about the mean of consecutive legs. No more than three consecutive legs were flown consecutively so that meteorological conditions were relatively steady state.

flux	within leg variation (%)	leg to leg variation (%)
U_* (m/s)	25 – 40	5 – 20
H (W/m^2)	40 – 65	10 – 25
LE (W/m^2)	40 – 80	10 – 25
FCO_2 (mg/m^2/s)	15 - 155	0 - 100

9.4.2 THE SHOALING WAVE EXPERIMENT

During the Fall 1997 the Long-EZ aircraft was involved in studies to measure air-sea interactions within a shoaling zone. The study site was a region east of Duck, NC where the continental shelf extended approximately 80 - 90 km offshore (source: U. S. Army Waterways Experiment Station, Field Research Facility, Duck, NC). On this particular mission the aircraft was equipped with a three-laser array measuring distance to the sea surface. This array was deployed in order to collect sea surface

wave characteristic measurements using methods analogous to those used with wave wires at fixed points. Initial results from this study can be found in Sun et al. (1999) and Vogel et al. (1999).

9.4.2.1 Drag Coefficient variations

A principle goal of the Duck study was to address drag coefficient modulation within a shoaling region. It has been hypothesized for some time that relationships established for the atmospheric drag coefficient over a sea nearly in equilibrium with the forcings of atmospheric stress begin to break down in shoaling regions where surface waters "feel" the presence of the ocean floor. The bathymetry perpendicular to the coastline at Duck was such that the continental shelf extended eastward to approximately 80 km offshore. To first order, the ocean depth decreased nearly linearly from approximately 35 m at 80 km offshore to 20 m 10 km offshore. At distances less than 10 km the ocean depth decreased exponentially. Consequently, to investigate drag coefficient variations within a shoaling region, a transect approximately 100 km in length, perpendicular to the shoreline was flown repeatedly from a point 10 km west of Duck to a point 90 km offshore.

Figure 9.6 shows average values of the drag coefficient as a function of distance from shore. This particular case involved winds from the NNE producing a small onshore component in the winds. Note the relatively constant value of the drag coefficient at distances greater than approximately 20 km. For the open sea the neutral drag coefficient is usually parameterized as a function of wind speed at a 10 meter height. For example, Garratt (1992) gives the linear relation $C_{DN} = (a + b\,U_{10}) \times 10^{-3}$ with $a = 0.775$ and $b = 0.066$ for aerodynamically rough flow, i.e., wind speeds greater than about 4 m/s. Figure 9.6 shows heat and moisture fluxes of approximately 40 W/m^2 and 90 W/m^2 respectively indicating a stability regime that could be considered near neutral. Note the high correlation between these energy fluxes and the spatial variation of the air-sea temperature difference. Using this relationship, the observed 20 m wind speeds extrapolated to 10 meters of approximately 6 m/s shown in the Figure give values near 1.17×10^{-3}, in close agreement with drag coefficient values shown at distances greater than 20 km.

At distances less than 20 km, however, the drag coefficient values begin to increase significantly. Simultaneously, the 10 m wind speed decreases indicating that a variable or variables other than wind speed are influencing drag coefficient behavior. A number of investigators have proposed that wave age defined as the ratio of the wave phase speed c_p to u_*, has a significant influence on the drag coefficient within a shoaling zone (e.g. Kitaigorodskii 1973; Davidson 1974; Geernaert et al. 1986, 1987; Donelan 1990). Over the open sea, capillary waves determine to a large extent the roughness presented to the atmospheric flow and the sea surface wave phase speed is more in equilibrium with the surface stress. However, within shoaling regions there can be acceleration or deceleration of the atmospheric flow as well as surface waves becoming influenced by the ocean floor thus producing younger less developed waves. Efforts to extract wave age and other sea surface characteristics are proceeding at the time of this writing.

9.4.2.2 Wave Height Measurements

As stated above, the Long EZ aircraft was equipped with a downward pointing three-laser array measuring distances to the sea surface. This was in order to conduct seminal simultaneous investigations into atmospheric stress and sea surface interactions. In order to accurately determine wave height measurements from an airborne platform a transformation must be made between aircraft coordinates and earth coordinates. Since all position measurements of the aircraft are referenced to an antenna mounted on the probe ahead of the aircraft, the coordinate transformation was applied on the sum of two vectors: 1) a displacement vector from the antenna to each laser position on the aircraft, and 2) the distance vector (perpendicular to the centerline of the aircraft) from each laser to the sea surface. Mathematically this can be expressed by defining a laser displacement matrix LD and a laser measurement matrix LM :

$$LD = \begin{bmatrix} d_{1x} & d_{2x} & d_{3x} \\ d_{1y} & d_{2y} & d_{3y} \\ d_{1z} & d_{2z} & d_{3z} \end{bmatrix}, \qquad LM = \begin{bmatrix} 0 & 0 & 0 \\ 0 & 0 & 0 \\ L_1 & L_2 & L_3 \end{bmatrix} \tag{9-7}$$

where LD contains the three components of the distance from the antenna to each laser, and LM contains the distance measurements from the lasers to the ocean surface. A transformation matrix T can be derived:

$$T = \begin{bmatrix} \cos\alpha\cdot\cos\gamma+\sin\alpha\cdot\sin\beta\cdot\sin\gamma & -\sin\alpha\cdot\cos\beta & -\cos\alpha\cdot\sin\gamma+\sin\alpha\cdot\sin\beta\cdot\cos\gamma \\ \sin\alpha\cdot\cos\gamma-\cos\alpha\cdot\sin\beta\cdot\sin\gamma & \cos\alpha\cdot\cos\beta & -\sin\alpha\cdot\sin\gamma-\cos\alpha\cdot\sin\beta\cdot\cos\gamma \\ \cos\beta\cdot\sin\gamma & \sin\beta & \cos\beta\cdot\cos\gamma \end{bmatrix}$$

where α = heading, β = roll, and γ = pitch angle of the aircraft. The earth-coordinate transformed laser measurements LM_e is then generated through:

$$LM_e = \begin{bmatrix} L_{1xe} & L_{2xe} & L_{3xe} \\ L_{1ye} & L_{2ye} & L_{3ye} \\ L_{1ze} & L_{2ze} & L_{3ze} \end{bmatrix} = T\cdot(LD + LM)$$

Once the transformation is applied the wave heights can be resolved by operating on the vertical components of LM_e through removing the aircraft altitudes and high pass filtering the data.

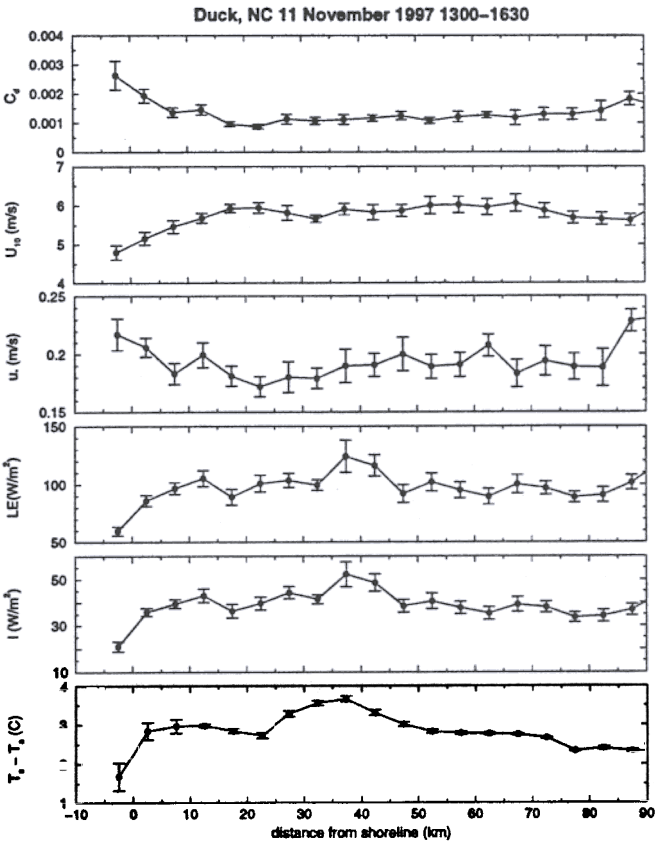

Figure 9.6 Aircraft measurements as a function of distance eastward from the Duck, N.C., shoreline. the wind has a slight onshore flow. In descending order. The panels show the drag coefficient, windspeed, friction velocity, latent heat flux, sensible heat flux, and air-sea temperature difference.

Figure 9.7 shows sample traces for all three lasers on 5 November 1997. The aircraft was flying approximately 60 km offshore with nominal ground speeds of 45 m/s. The upper plot shows traces over a slightly greater than 10 second period. The lower plot shows a subset of these traces over a 1 second period. In the upper plot surface ocean waves are readily apparent with spatial scales on the order of 10 m. It is important to note that due to the limitations in determining the absolute aircraft altitude from the GPS system used, wave heights could not be resolved to better than 20 cm. However, the relative measurements from the 3 lasers have millimeter accuracy and current efforts include using the apparent wave slope in conjunction with a Ka-band radar to approximate surface roughness (D. Vandemark personal communication).

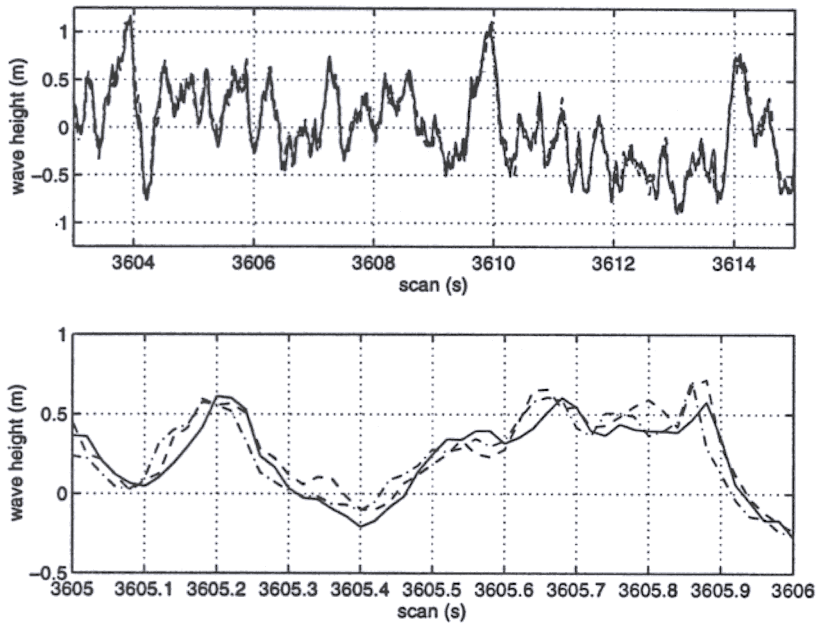

Figure 9.7 Laser scans of wave-height for a 10-second period (upper plot) and a 1-second period (lower plot) for aircraft speed of 45 m/sec. See text for details.

9.5 Conclusion

The Long-EZ aircraft has thus far filled an important need in achieving difficult spatial measurements within the marine atmospheric surface layer. The system is complex and the potential for error is greater than flux measurement systems mounted at fixed points. Thus, there has been a continuous effort to perform detailed calibrations and to streamline data acquisition and instrument interfacing. A primary limiting factor of the system has been the resolution of the GPS position measurements. As mentioned in the discussion on determining sea surface heights from a laser altimeter array, the resolution of the aircraft position was at best 20 cm. However, recent additions of improved GPS receivers are expected to reduce these uncertainties at least in half. As instrument technology and computer processing speeds improve it is expected that this airborne platform will continue to reveal exciting phenomena relating to air-sea interaction and the turbulence structure above the sea surface.

9.6 References

Auble, D.R., Meyers, T.L. (1990) An H_20 and CO_2 open-path gas analyzer for use with eddy flux systems. *Boundary-Layer Meteorology*, **59**, 243 – 256.

Crawford, T.L., McMillen, R.T., Dobosy, R.J. (1990) Desciption of a 'generic' mobile flux platform using a small airplane. *NOAA Technical Memorandum ERL ARL – 184*, 81 pp.

Crawford, T.L., Dobosy, R.J. (1992) A sensitive fast-response probe to measure turbulence and heat flux from any airplane. *Boundary-Layer Meteorology*, **59**, 257 – 278.

Crawford, T.L., McMillen, R.T., Dobosy, R.J., MacPherson, I. (1992) Correcting airborne flux measurements for aircraft speed variation. *Boundary-Layer Meteorology*, **66**, 237 – 245.

Crawford, T.L., Dobosy, R.J., McMillen, R.T., Vogel, C.A., Hicks, B.B. (1996) Air-surface exchange measurement in heterogeneous regions: extending tower observations with spatial structure bserved from small aircraft. *Global Change Biology*, **2**, 275 – 286.

Donelan, M. (1990) Air-sea interaction. *Ocean Engineering Science*, B. LeMehaute and D. M. Hanes, eds, John Wiley and Sons, 239 – 291.

Dejardins, R.L., Brach, E.J., Alno, P., Schuepp, P.H. (1982) Aircraft monitoring of surface carbon dioxide exchange. *Science*, **216**, 733 – 735.

Dejardins, R.L., MacPherson, J.I., Schuepp, P.H., Karanja, F. (1989) An evaluation of aircraft flux measurements of CO2, water vapor, and sensible heat. *Boundary-Layer Meteorology*, **47**, 55 – 69.

Garratt, J.R. (1992) *The Atmospheric Boundary Layer*. Cambridge University Press, Cambridge, UK, 316 pp.

Geernaert, G.L., Katsaros, K.B., Richter, K. (1986) Variation of the drag coefficient and its dependence on sea state. , *Journal of Geophysical Research*, **91**, 7667 – 7679.

Geernaert, G.L., Larsen, S.E., Hansen, F. (1987) Measurements of the wind stress, heat flux, and turbulence ntensity during storm conditions over the North Sea, *Journal of Geophysical Research*, **92**, 13,127 – 13,139.

Hacker, J.M., Scherdtfeger, P. (1988) The FIAMS research aircraft description. *Technical report no. 8*, Flinders Institute for Atmospheric and Marine Sciences, The Flinders University of South Australia, SA, 5042.

Kanemasu, E.T., Wesely, M.L., Hicks, B.B., Heilman, J.L. (1979) Techniques for calculating energy and mass fluxes. In Modification of the Aerial Environment of Crops, ASAE Monograph No. 2, (Edited by B. J. Barfield and J. F. Gerber), *American Society of Agricultural Engineers*, St. Joseph, MO, 156-182.

Kiaigorodskii, S.A. (1973) The physics of air-sea interaction, translated from Russian, Israel Program for Scientific Translations, Jerusalem, 273 pp.

Lenshow, D.H. (1972) The measurement of air velocity and temperature using the NCAR Buffalo aircraft measuring system. *NCAR-TN/EDD-74*.

Lenshow, D.H., Delany, A.C., Stankov, B.B., Stedman, D.H. (1980) Airborne measurements of the vertical flux of ozone in the boundary layer. *Boundary-Layer Meteorology*, **19**, 249 – 265.

Lenshow, D.H., Pearson Jr., R., Stankov, B.B. (1981) Estimating the ozone budget in the boundary layer by use of aircraft measurements of ozone eddy flux and mean concentration. *Journal of Geophysical Research*, **86**, 7291 – 7297.

Smith, S.D., Fairall, C.W., Geernaert, G.L., Hasse, L. (1996) Air-sea fluxes: 25 years of progress. *Boundary-Layer Meteorology*, **78**, 247 – 290.

Sun, J., L. Mahrt, Vickers, D., Wong, J., Crawford, T., Vogel, C., Dumas, E., Mourad, P., Vandemark, D. (1999) Air-sea interaction in the coastal zone. *13th Symposium on Boundary Layers and Turbulence*, American Meteorological Society, 10 – 15 January 1999, Dallas, TX, 343 – 345.

Vogel, C.A., Crawford, T.L. (1996) Temporal and spatial variabilities of heat, moisture, CO_2 and momentum flux densities above the air-sea interface. *1996 Ocean Sciences Meeting*, American Geophysical Union, 12 – 16 February 1996, San Diego, CA.

Vogel, C.A., Crawford, T.L. (1997) Dissipation measurements in the marine atmospheric surface layer. *12th Symposium on Boundary Layers and Turbulence*, American Meteorological Society, 28 July – 1 August 1997, Vancouver, BC, Canada, 310 – 311.

Vogel, C.A., Crawford, T.L., Sun, J., Mahrt, L. (1999) Spatial variation of the atmospheric drag coefficient within a coastal shoaling zone, *13th Symposium on Boundary Layers and Turbulence*, American Meteorological Society, 10 – 15 January 1999, Dallas, TX, 347 – 348.